PTEP

Prog. Theor. Exp. Phys. **2012**, 02B002 (17 pages)
DOI: 10.1093/ptep/pts019

Beam commissioning and operation of the J-PARC linac

Masanori Ikegami

Accelerator Laboratory, High Energy Accelerator Research Organization, 1-1 Oho, Tsukuba, Ibaraki 305-0801, Japan
E-mail: masanori.ikegami@kep.jp

Received June 13, 2012; Accepted July 2, 2012; Published September 28, 2012

J-PARC (the Japan Proton Accelerator Research Complex) is a high intensity proton accelerator facility aiming to realize 1 MW class beam power. The J-PARC linac is the injector for the accelerator complex with a current designed beam power of 36 kW. The beam commissioning of the J-PARC linac was started in November 2006, and its user operation began in December 2008. Since then, beam commisioning has been performed to increase the beam power while mitigating the accompanying beam loss. In the beam loss mitigation study to date, we have revealed that beam loss in the J-PARC linac is mainly caused by electron stripping of negative hydrogen ions in residual gas scattering. As of May 2012, the linac beam power for nominal operation is 13.3 kW, which is about one-third of the designed beam power. Although the massive earthquake in March 2011 forced us to shut down for nearly nine months, we resumed beam operation in December 2011 and user operation in January 2012. Subsequently, in March 2012, we retained the same beam power as just before the earthquake.

1. Introduction

J-PARC (the Japan Proton Accelerator Research Complex) is a high intensity proton accelerator facility located at Tokai village in Japan [1]. It aims to provide 1 MW class beam power for various applications ranging from particle physics to life and material sciences. A cascade ring configuration is used for the J-PARC accelerator to accommodate various needs for multiple energy ranges. The J-PARC accelerator consists of a 181 MeV linac, a 3 GeV RCS (rapid cycling synchrotron), and a 30 GeV MR (main ring) [2]. A 3 GeV beam from the RCS is provided to both the MR and the MLF (material and life science facility). The MLF accommodates a neutron target and a muon target. In addition, the MR has two target stations for fast-extracted and slow-extracted beams, respectively. The linac serves as an injector to the RCS without its own user facility. The designed peak current for the J-PARC linac is 30 mA, the macro-pulse width 0.5 mA, and the repetition rate 25 Hz. We assume beam chopping to mitigate the beam loss in the RCS, as discussed in a later section, and the designed output beam power from the linac is 36 kW, taking the chopper beam-on duty factor into consideration. This linac beam power corresponds to a beam power of 600 kW from the RCS. The linac beam power is to be upgraded to 133 kW to achieve an RCS beam power of 1 MW, as discussed below.

Since user operation started in December 2008, the linac beam power has been gradually increased. As of May 2012, the J-PARC linac is operating with a peak current of 15 mA. The beam for the MLF is accelerated with a pulse width of 0.38 ms and a repetition of 25 Hz, which corresponds to a linac beam power of 13.3 kW and an RCS beam power of 200 kW. We have a switching magnet after the RCS,

with which the beam destination for each pulse can be selected between the MLF and MR. Using this switching magnet, a train of eight RCS bunches is delivered to the MR with its operation cycle. The timing system is designed so that we can adopt different pulse structures for the MLF and MR, and we operate with a macro-pulse width of 0.5 ms for the pulses for the MR in the case of fast extraction. If we continue 25 Hz operation with this beam parameter, the RCS beam power would reach 300 kW. Namely, we are providing a 300 kW equivalent beam to the MR without any notable problem. While the available beam power in a high intensity accelerator is often limited by the residual radiation level to sustain hands-on maintenance, this beam power is realized with a reasonable margin for the residual radiation level in the linac. Actually, the highest radiation dose several hours after the beam shutdown of 13.3 kW operation is typically 1 mSv/h on the chamber surface and less than 0.1 mSv/h at one foot distance. This is sufficiently lower than the widely accepted practical hands-on maintenance limit of 1 mSv/h at one foot distance [3]. The present beam power is determined from various factors, including the stability of the linac front-end, the beam loss in MR, and the durability of the neutron target. Namely, we are currently increasing the beam power, keeping pace with the downstream accelerators and user facilities. In this regard, it would be reasonable to say that we are in beam commissioning while user operation is conducted in parallel.

In this paper, we present characteristic features in the beam commissioning and operation of the J-PARC linac. As a small fraction of beam loss can prevent us from performing hands-on maintenance of accelerator components, it is of essential importance to mitigate the beam loss in a high intensity linac. To this end, accurate tuning of operating parameters is assumed to be essential. It is also assumed to be indispensable to conduct beam studies to identify the beam loss mechanism and to devise a countermeasure based on the experimental measurement. Due to limitations of spaces, we do not entirely cover the elaborated beam commissioning procedures in this paper. Instead, we try to highlight the distinctive features of beam commissioning for the J-PARC linac, taking some characteristic topics to the latest high intensity proton linacs. We had a massive earthquake in March 2011, and the beam commissioning and operation of the J-PARC linac were seriously affected by the resultant damage. After significant efforts at restoration, the beam operation of the J-PARC accelerators was resumed in December 2011 and the user operation in January 2012. In this paper, we also briefly describe the latest status of the J-PARC linac after restoration after the earthquake.

This paper is organized as follows. Before discussing the beam commissioning of the J-PARC linac, we outline the design of the J-PARC linac and its characteristic features in Sect. 2. In Sect. 3, we divide the beam commissioning into two stages. Then, we discuss two distinctive topics for each stage. After presenting the status after the earthquake in Sect. 4, a summary is given in Sect. 5.

2. Linac design overview

2.1. Linac design and layout

Negative hydrogen ions instead of protons are accelerated with the J-PARC linac, because the charge-exchange injection scheme [4] is used at the RCS. In this scheme, the accelerated negative hydrogen ions are charge-exchanged to protons with a stripper foil at the RCS injection. This injection scheme has been adopted to enable effective beam stacking at the injection, and hence to achieve a higher beam intensity at the RCS. As the mass of a negative hydrogen ion is close to that of a proton, we can adopt proton linac structures for the linac. Accordingly, a linac for negative hydrogen ions is often called a "proton linac". We follow this usage in this paper and call the J-PARC linac a proton linac, although beam loss circumstances in a negative hydrogen ion linac are significantly different from those in a proton linac, as discussed in a later section. As is the case in a conventional proton

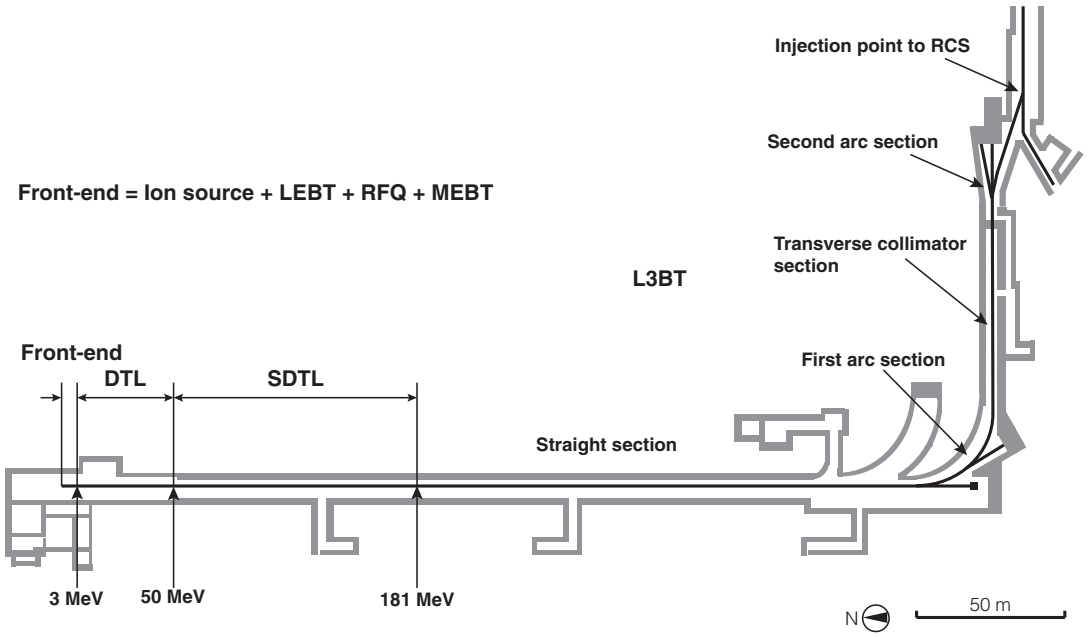

Fig. 1. Schematic layout of the J-PARC linac (top view).

linac, we use a few different accelerating structures in the J-PARC linac, because the particle velocity changes significantly in the assumed energy range. This requires us to adopt an optimum accelerating structure for each particle velocity range.

As shown in Fig. 1, the J-PARC linac consists of a 50 keV negative hydrogen ion source, a 3 MeV RFQ (radio frequency quadrupole linac), a 50 MeV DTL (drift tube linac) of Alvarez type, and a 181 MeV SDTL (separate-type DTL). A combination of an RFQ and a DTL is a conventional choice for the front-end part of a modern proton linac, while the SDTL was specially devised for the J-PARC linac [5]. The RF power efficiency, or shunt impedance, of a DTL is lower with higher particle velocity. Then, it is usual to switch to a CCL (coupled cavity linac) at some energy, introducing a frequency jump. However, the shunt impedance around the transition tends to be low, because a CCL has a lower shunt impedance with smaller β. Here, β denotes the particle velocity scaled by the speed of light. The SDTL is used to remedy this shortcoming, having a higher shunt impedance at the transition β range. In contrast to a DTL accommodating a quadrupole magnet for transverse focusing in its drift tube, the SDTL has empty drift tubes with external quadrupole magnets in inter-tank spaces. Eliminating the quadrupole magnets from the drift tubes gives the SDTL a greater flexibility in drift tube geometry, which enables us to realize design optimization for higher shunt impedance. It should also be noted that the transverse focusing lattice of an SDTL is similar to that of a CCL, which is advantageous in smoothly connecting to a higher β structure.

The output beam from the SDTL is delivered to a 3 GeV RCS through a beam transport line called an L3BT (linac-to-3-GeV RCS beam transport). We have two debuncher cavities and a transverse collimator system in the L3BT. The transverse collimator system is prepared to reduce the beam loss around the injection point by eliminating the transverse halo component [8]. In this collimator system, the halo component is charge-exchanged to protons with stripper foils and then transported down to a dedicated beam dump. While we do not use this collimator system in nominal operation with the current beam power level, it would be useful in mitigating the beam loss in the injection region after future increases in the beam power. In mitigating the beam loss in the RCS, elaborated control

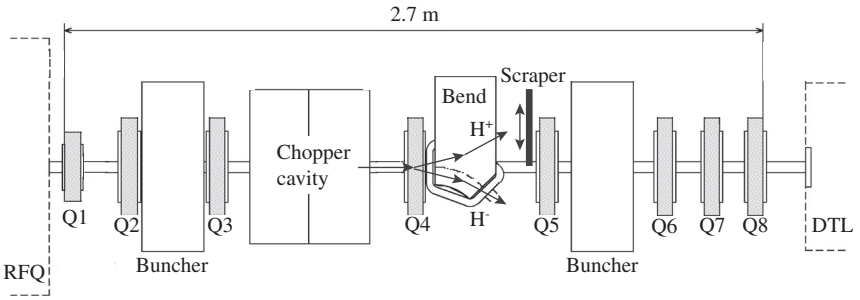

Fig. 2. Schematic layout of the MEBT (top view). The eight quadrupole magnets in the MEBT are shown as Q1 to Q8. The separated orbits for protons and negative hydrogen ions discussed in Sect. 3.3 are also schematically shown with arrows.

of the RF parameters is essential [9]. To realize RF tuning, the linac beam should have optimized momentum spread with sufficiently suppressed momentum centroid jitter. To realize the longitudinal beam properties in the RCS injection, we have a two-cavity debuncher system in the L3BT. We have adopted the so-called "separate-function configuration" [10] for this debuncher system, which was devised for the J-PARC linac. In this configuration, the first debuncher cavity is used solely to correct the beam centroid energy jitter in a passive manner. Meanwhile, the second debuncher cavity is used exclusively to control the momentum spread at the RCS injection without affecting the jitter correction with the first cavity. This configuration offers flexible control of momentum spread at the RCS injection without sacrificing the momentum jitter correction.

The J-PARC linac has two more beam transport lines with specific functions. One is an MEBT (medium energy beam transport) connecting the RFQ and DTL. The main purpose of this line is to realize the transverse and longitudinal matching between the RFQ and DTL. To this end, the MEBT is equipped with two buncher cavities and eight quadrupole magnets with various pieces of beam diagnostic instrumentation, as shown in Fig. 2. All the quadrupole magnets in the MEBT have additional winding to steer the beam in both the horizontal and vertical directions. Beam chopping is also an important function of the MEBT. As shown in Fig. 3, the linac beam has an additional pulse structure called a "medium pulse structure" to mitigate the beam loss in the RCS. The medium pulse structure is formed by eliminating, or chopping, some temporal portion of the beam with the RF chopper system. The RF chopper system consists of an RF chopper cavity and a scraper, both of which are installed in the MEBT [6,7]. The RF chopper cavity is an RF deflector with a TE_{11}-like mode with the same RF frequency as the RFQ. While the RF chopper cavity is on, the beam is deflected horizontally to be absorbed by a scraper downstream. Meanwhile, the beam transmits through the chopper system with the RF chopper cavity off. Then, it is possible to form an arbitrary medium pulse structure by controlling the gate signal for the RF power source of the RF chopper cavity. If a beam is injected into the RCS without chopping, some portion of the beam spills out of the RF bucket and is finally lost in the RCS. To mitigate the beam loss, the beam is chopped so that we do not inject the beam around the edge of the RF bucket. The chopping gate frequency is synchronized with the RF system in the RCS with a frequency of about 1 MHz, and the chopper beam-on duty factor is 56% in design. While a chopper system is often assumed in recent high power proton injector linacs, most of them are based on a so-called slow wave kicker, where the pulsed electrical wave propagates along the kicker, being synchronized with the particle velocity [11]. For a slow wave kicker, it is often a technical challenge to develop a pulsed power source satisfying the required specifications for the

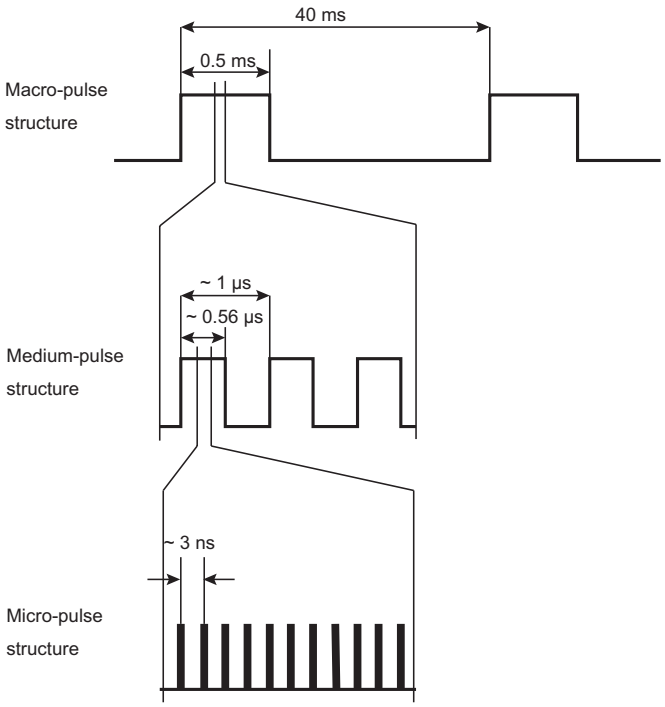

Fig. 3. A nonscaled schematic for the beam pulse structure in the J-PARC linac.

chopper system. Meanwhile, we adopt an RF deflector for the chopper system, taking advantage of the established technique of RF power sources using a solid-state RF amplifier. This provides us with the capability of stable operation and flexible manipulation of the medium pulse structure. Our chopper system operates stably during nominal operation and its significantly low beam extinction ratio has been confirmed experimentally [12].

The other beam transport line is an LEBT (low energy beam transport) between the ion source and the RFQ. The main function of the LEBT is to conduct transverse beam matching to the RFQ, and we use solenoid focusing in this line instead of electrostatic focusing. It should be noted that we can take advantage of the charge neutralization effect [13] with solenoid focusing to suppress the space charge effect in this line.

The main parameters for the J-PARC linac are summarized in Table 1. It should be noted that all the RF cavities in the J-PARC linac are normal conducting with the same operating frequency of 324 MHz.

2.2. Upgradability

The J-PARC linac is currently operating with an output energy of 181 MeV and a designed peak current of 30 mA. Thereby, we can reach an RCS output beam power of 600 kW. To realize 1 MW beam power from RCS, we plan to have both energy and intensity upgrades for the linac. In the intensity upgrade, we plan to replace the ion source and the RFQ to deliver a peak current of 50 mA. As the current RFQ is optimized for 30 mA peak current, a new RFQ optimized for 50 mA is currently under construction. As for the ion source, we are developing a cesium-seeded RF ion source to replace the current cesium-free LaB_6 filament ion source [14]. In the energy upgrade, the linac output energy will be increased to 400 MeV by adding an ACS (annular coupled structure linac) [15] after the SDTL. The ACS is a variation of the CCL with emphasis on the axial symmetry of the RF field.

Table 1. Main parameters for the J-PARC linac.

	Parameter	Value
General	Ion species	Negative hydrogen ions
	Output energy	181 MeV
	Macro-pulse width	0.5 ms
	Repetition rate	25 Hz
	Chopper beam-on duty factor	56%
	Beam power	36 kW
RFQ	Type	Four-vane
	RF frequency	324 MHz
	Input energy	0.05 MeV
	Output energy	3 MeV
	Number of tanks	1
	Number of tanks per klystron	1
	Vane voltage	1.8 Kilpatrick limit
	Wall loss power	0.3 MW
	Length	3 m
DTL	Type	Alvarez
	RF frequency	324 MHz
	Input energy	3 MeV
	Output energy	50 MeV
	Number of tanks	3
	Number of cells per tank	76, 43, 27
	Number of tanks per klystron	1
	Average accelerating field	2.5 to 2.9 MV/m
	Synchronous phase	-30°
	Total wall loss power	3.3 MW
	Total length	27 m
SDTL	Type	Alvarez
	RF frequency	324 MHz
	Input energy	50 MeV
	Output energy	181 MeV
	Number of tanks	30
	Number of cells per tank	5
	Number of tanks per klystron	2
	Average accelerating field	2.5 to 3.7 MV/m
	Synchronous phase	-27°
	Total wall loss power	14.7 MW
	Total length	84 m

The ACS has an RF frequency of 972 MHz with a three-fold frequency jump from the SDTL. The space charge effect in the RCS injection is increased with the intensity upgrade, and it could limit the obtainable beam power. To suppress the space-charge effects to a tolerable level, it is necessary to increase the injection energy. In this regard, the energy upgrade is essential for the beam power upgrade of J-PARC. Currently, we plan to accommodate these upgrades in the summer of 2013; the fabrication of the ACS cavities has mostly been completed and awaits their installation.

For further future upgrades, all the RF cavities including the ACS are designed to sustain 50 Hz operation. In 50 Hz operation, 25 Hz of the beam is supposed to be provided to RCS and the other 25 Hz is used for other purposes, utilizing a switching magnet. As the RF sources are also designed to accommodate 50 Hz operation, this upgrade can be realized with reasonable investments in the utility, branch beam line, and possibly chopper system upgrade. As discussed above, we assume a three-fold frequency jump between the SDTL and the ACS, instead of the often-used two-fold frequency jump. This choice secures the possibility for simultaneous acceleration of protons and negative hydrogen

ions. Although it would possibly require an upgrade in the RF sources and the front-end, this choice provides further potential for future upgrades.

2.3. Characteristic features

One of the characteristic features of the J-PARC linac is the use of an electromagnet quadrupole for the DTL. Although an electromagnet quadrupole magnet used to be a nominal choice for a DTQ (drift tube quadrupole), a PMQ (permanent magnet quadrupole) has recently been becoming a common choice. A compact PMQ enables the use of higher RF frequency for a DTL, which is advantageous in terms of the RF power efficiency. Also, a PMQ is often used in recent proton linacs for transverse focusing, sacrificing the tunability of the quadrupole gradient [20–22]. It should also be noted that the higher RF frequency enables the adoption of a klystron for the RF source, which also improves the cost efficiency of the RF system. In the J-PARC linac, however, we use an electromagnet for the DTQ, emphasizing the importance of flexibility in the transverse tuning. Compatibility between the electromagnet DTQ and a klystron-based RF system has been realized by the invention of a DTQ based on a compact electroformed hollow coil, a so-called "Sakae coil" [16]. The choice of 324 MHz for the RF frequency has been made to realize the electromagnet DTQ and the klystron-based RF system simultaneously, which required the development of a klystron with the new frequency dedicated to the J-PARC linac.

As for the transverse focusing configuration along the linac, the so-called "equipartitioning setting" has been proposed [17,18]. In this setting, the quadrupole strength is determined so that the beam temperatures in the transverse and longitudinal directions are balanced, to avoid heat transfer between these degrees of freedom. There has been concern that the heat transfer could result in emittance growth in a high intensity linac. Although there is an argument that the avoidance of longitudinal–transverse coupling resonances is more essential than satisfying the equipartitioning condition [19], the equipartitioning condition is a sufficient condition for resonance avoidance. In the J-PARC linac, the quadrupole magnets are designed so that the equipartitioning condition can be realized with a reasonable margin, and we adopt the equipartitioning setting for the usual operation. It should be noted that the quadrupole gradient satisfying the condition depends on the assumed beam current and emittance, and it is not obvious whether we can accurately predict the beam emittance before actually constructing the accelerator. Adopting electromagnet quadrupoles for the entire linac, the equipartitioning condition can be satisfied for various beam conditions in the J-PARC linac. This feature is particularly important to realize sufficient optimization on each phase of intensity upgrade and to retain reasonable flexibility for future upgrades. It is also possible to try different quadrupole settings to compare the resultant beam quality with the equipartitioning setting, which would provide us with valuable information for the design of future high intensity proton linacs.

As most recent high intensity proton linacs use or planning to use superconducting RF cavities, especially for their high energy parts [20–22], the full-scale adoption of normal conducting structures is also a distinguishing characteristic for the J-PARC linac. In a normal conducting structure, the geometrical β of the cavities almost exactly follows the evolution of particle β whereas coarse grouping of it is usually adopted for a superconducting structure. Here, the geometrical β is the β value of a particle that best fits the cell geometry. This design difference is generally introduced to maximize the cost advantage of the superconducting structure. The larger mismatch between the geometrical and particle β due to the grouping introduces a larger phase slip, or cell-to-cell variation of the synchronous phase, in a superconducting cavity. While the geometrical β grouping is designed

to suppress the unfavorable effect from the phase slip to below a tolerable level, a larger variation of the longitudinal focusing force is generally introduced in a superconducting linac. In contrast, the longitudinal focusing force is smoother in a normal conducting structure, which is expected to help suppress the longitudinal emittance growth during the acceleration. It should also be noted that the choice of the normal conducting structure is strongly related to the use of the equipartitioning setting. As the assumed accelerating gradient is significantly higher in a superconducting linac, it is often hard to accommodate transverse focusing strong enough to match the longitudinal one. Thus, it is often difficult to satisfy the equipartitioning condition with a superconducting linac while fully using its cost advantage.

As is readily seen in this section, the design emphasis is consistently put on realizing a high quality beam in the J-PARC linac. To realize a high quality beam, design choices are made to avoid potentially unfavorable effects and to sustain sufficient tunability to secure the capability of precise tuning. Emphasis is also put on having flexible upgradability. The design is such that a high quality beam could be obtained even after the upgrade with sufficient margin for its tunability.

3. Beam commissioning and operation

As seen in the previous section, we have significant flexibility in the operation parameters for tuning in the J-PARC linac. With this design strategy, accurate tuning of operation parameters is of particular importance. We here divide the beam commissioning of the J-PARC linac into two stages. One is the initial commissioning stage, where we confirm proper functioning of the linac components and establish beam operation with the minimum beam power to start the beam commissioning of downstream accelerators. In parallel, we try to achieve tuning that is as accurate as possible at this stage in preparation for the next stage. The other is the stage for beam-power reinforcement, where we increase the beam power while suppressing the beam loss and the residual radiation doses.

The first stage of beam commissioning involves beam tuning to determine the basic operating parameters, e.g., phase and amplitude set-point for each RF source, excitation current for each quadrupole magnet, and excitation current for each steering magnet. In this stage, we first tried to achieve acceleration to the designed beam energy with crude tuning for the RF parameters. After achieving the acceleration, we focused on confirming the functioning of beam diagnostics utilizing the accelerated beam, because this is the key to accurate tuning. Subsequently, we proceeded to finer tuning of the beam parameters with a limited beam current and beam duty factor. Thereby, we were able to operate the J-PARC linac with low beam power without any notable difficulties. After completing the beam commissioning of this stage, we started to provide a low-power beam to the RCS for its initial beam commissioning [23–25].

The second stage of the linac beam commissioning started with the commencement of high duty-factor operation for users, at which visible residual radiation arose. It should be noted that it is difficult to quantitatively correlate the beam loss monitor signal with the residual radiation dose without actually conducting high duty-factor operation. In the second stage, the emphasis of the beam commissioning naturally shifts to beam power ramp-up while mitigating the beam loss and resultant residual radiation. In particular, identification of the beam loss mechanism and devising a cure for it are crucial issues. This tuning was conducted in the intervals between user operation, and the beam power for user operation was increased as the beam loss mitigation study advanced.

Historically speaking, the first stage of beam commissioning started in November 2006 and continued until June 2007. We started to provide the beam to the RCS for its beam commissioning in October 2007. The second stage of beam commissioning, or the user operation to neutron users,

started in December 2008. As we are aiming at further beam power reinforcement, as discussed above, it would be fair to say that we are currently in the second stage of beam commissioning.

In this section, we take up four distinctive topics in the following subsections to highlight the characteristic features of beam commissioning in the J-PARC linac. First, we discuss two tuning procedures characteristic of the first stage of beam commissioning. Then, we present two studies regarding beam loss mitigation in the second stage.

3.1. Phase–amplitude scan tuning

Beam-based RF set-point tuning is a crucial step in the first stage of beam commissioning, where we find an adequate set-point for the RF phase and amplitude for each RF source. Excess tuning error for the RF set-point results in emittance growth in both the transverse and longitudinal directions, which may eventually lead to beam loss at the injection point to the RCS and other locations. The required accuracy for the tuning is 1 degree for the phase set-point and 1% for the amplitude set-point. The RF set-point is supposed to be adjusted for one RF source at a time from the upstream end. We use the so-called "phase–amplitude scan method" for this tuning [26,27]. In this method, the phase set-point is scanned while monitoring the output energy from the cavity undergoing tuning. The beam energy is measured with the TOF (time-of-flight) method using two downstream beam phase monitors, or FCTs (fast current transformers). The dependence of the output beam energy on the RF phase set-point, or the phase scan curve, is obtained for various RF amplitude settings. Then, those phase scan curves are compared with a simulated curve to find the adequate set-points for the RF phase and amplitude. This tuning scheme is used for all the RF cavities except for the RFQ and chopper cavities.

In the case of a single gap cavity, the resultant phase scan curve would be a sinusoid, as is the case with the buncher cavities. In this case, the adequate set-point can easily be found because the observed beam energy modulation is directly connected to the cavity amplitude. Then, the phase of the sinusoid corresponds to the synchronous phase. However, cell-to-cell phase slip in a multi-cell cavity distorts the phase scan curve in a specific way in each cavity. In the case of the SDTL, where 10 cells, or 10 RF gaps, are fed by a klystron, the phase scan curve looks like a distorted sinusoid, as seen in Fig. 4. Then, it is necessary to conduct a phase scan over 360° to find the energy modulation amplitude with sufficient accuracy. Subsequently, adequate RF phase and amplitude set-points are found to fit the reference curve obtained with the IMPACT model [28]. Meanwhile, the DTL has 27 to 76 cells in each tank. This large number of cells significantly distorts the phase scan curve in a very sensitive way to the RF amplitude. In addition, the beam transmission efficiency drops with a phase setting too far from the designed value. Thus, we adopt a narrower phase scan range for the DTL to determine the RF amplitude. An adequate scanning range for the phase scan could be found with a crude phase scan monitoring the beam transmission efficiency. The principle of this tuning scheme is rather straightforward. However, it should be noted that this tuning scheme with sufficient accuracy become virtually available only recently after the phase scan with sufficiently wide and flexible range has been realized by the adoption of digital feedback to the low-level RF control system [29].

3.2. Transverse matching

Another crucial step in the first stage of beam commissioning is transverse matching, where the quadrupole strength is adjusted to make the transverse beam envelope smooth. The transverse mismatch and the resulting beam envelope oscillation are known to generate a beam halo through a

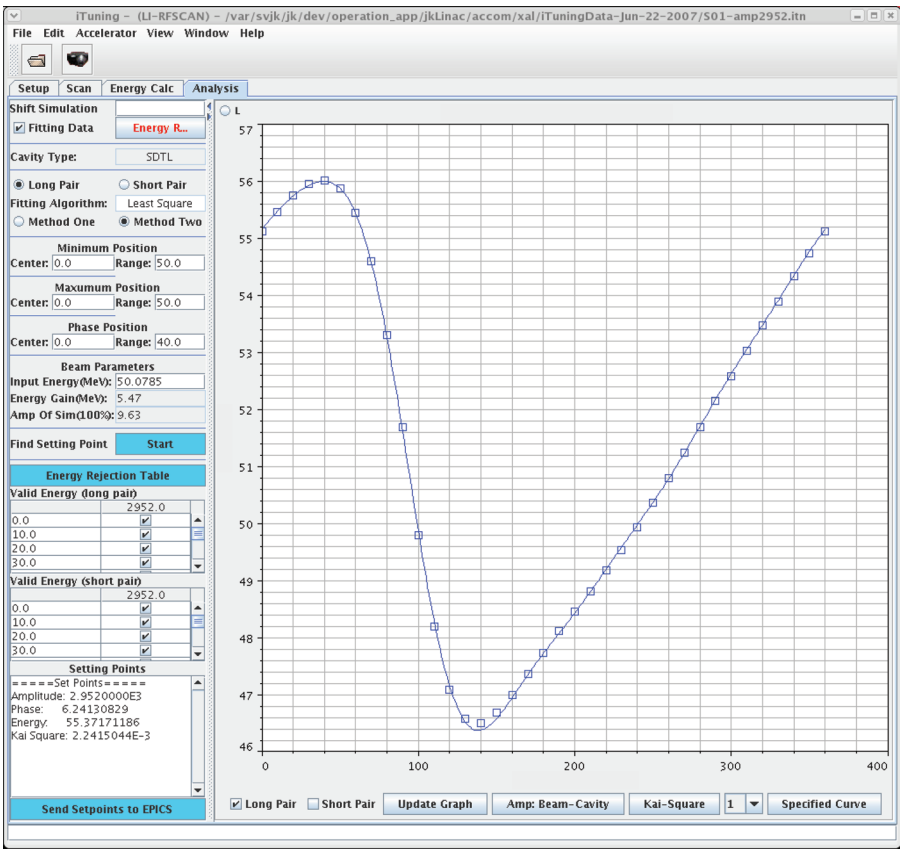

Fig. 4. A snapshot of the application software to conduct phase scan tuning. The obtained phase scan curve for the first SDTL module is shown with the phase setting as the horizontal axis and the measured energy as the vertical axis. The range for the horizontal axis is from 0 to 400°, and that for the vertical axis is from 46 to 57 MeV. In this plot, the measured output energy is shown with circle markers, and the simulated result with IMPACT is shown with a solid line. The software was developed with XAL.

particle–core resonance, which is considered to be a possible cause of beam loss in a high intensity linac [30–34]. Therefore, accurate transverse matching is assumed to be essential in mitigating the beam loss. It should be noted that the halo generated in this mechanism might not be lost in a linac with realistic mismatch, because its extent is known to be self-limiting and the linac aperture is designed to accommodate the extent with a reasonable margin. However, the developed halo could miss the charge-exchange foil at the RCS injection, inducing excessive beam loss in the injection area.

As discussed above, the strengths of the quadrupole magnets in the J-PARC linac are determined to satisfy the equipartitioning condition. The beam envelope basically evolves smoothly, because the quadrupole strength is smoothly varied to satisfy the equipartitioning condition. However, we have some transitions in the linac to accommodate different structures for respective β ranges, at which the lattice structure abruptly changes. We need to adjust the strengths of some quadrupole magnets to realize smooth matching at these transitions, and the beam-based adjustment for them is the objective of this tuning.

We have four transitions in the J-PARC linac and three in the L3BT, where transverse matching is assumed. Transverse matching is performed for one matching point at a time from the upstream end. We adopt a transverse matching scheme utilizing an array of periodically placed beam profile

monitors in most of the matching points [35–37]. In this scheme, we have four or more transverse beam profile monitors, or wire scanners, periodically placed at each matching point. Then, we specify four quadrupole magnets for each matching point, which are located immediately upstream of the corresponding wire scanner array. The strengths of the knob quadrupole magnets are adjusted so that we have the same beam widths as the wire scanners. We need three wire scanners to perform transverse matching in this scheme, and the remaining ones are basically prepared for redundancy. The degree of mismatch is often characterized with a so-called "mismatch factor". We here define the mismatch factor as the difference between the maximum and the minimum of the measured beam widths scaled by their average. Then, the tolerable limit we set for the mismatch factor is 20% to suppress the halo generation to a reasonable level. In this tuning, we use the XAL model [38] to predict the optimum quadrupole strength from the measured beam widths. After setting the quadrupole strengths to the predicted values, we perform a confirmation measurement with wire scanners. After a few iterations, we find adequate quadrupole strengths, which provide a mismatch factor of typically 10%. An example for the transverse matching result is shown in Fig. 5, where the beam envelopes are calculated to fit the measured beam widths before and after tuning. It is readily seen in this figure that the expected beam envelope is significantly smoother after matching.

3.3. Proton loss mitigation

Immediately after we started high-duty factor operation for users in December 2008, we experienced a relatively high radiation dose at the first bending magnet in the L3BT. The highest radiation dose at the yoke surface was 0.2 mSv/h after operation with a linac beam power of 0.3 kW. The observed residual radiation was significantly high considering the low beam power, and it could have been an obstacle for beam power reinforcement. Close observation of the radiation dose distribution at the bending magnet revealed that the dose was the highest at a location symmetrical to the beam exit with respect to the injection beam axis. This observation indicates that the radiation was induced by protons with almost the designed output energy of 181 MeV.

The protons are supposed to be generated in double electron stripping of negative hydrogen ions. There are supposed to be two possible locations for the proton generation of this energy. One is the straight section after the SDTL exit, and the other is the LEBT. It is obvious that the protons generated after the SDTL have an energy close to 181 MeV. It should be noted that the protons generated in the LEBT can be captured by the RFQ and then accelerated to the designed energy with the opposite RF phase to the negative hydrogen ions. The double electron stripping is supposed to be caused by scattering by the residual gas in both cases. Considering the observed vacuum pressure level and the corresponding cross section for the double electron stripping, we concluded that stripping in the LEBT was more likely to be the cause of proton generation.

Based on this supposition, we set up a chicane orbit in the MEBT to eliminate the proton component at an energy of 3 MeV [39]. In this chicane orbit, the negative hydrogen ion beam is horizontally bumped with steering magnets and a bending magnet. Then, the oppositely deflected protons are eliminated by a scraper originally placed for beam chopping. The separated beam orbits are schematically shown in Fig. 2. In a beam experiment, we set up the chicane orbit and we gradually installed the scraper to remove protons. As is readily seen in Fig. 6, the chicane orbit was confirmed to be very effective in reducing the beam loss at the first bending magnet with a slight decrease in the beam transmission for negative hydrogen ions. This showed that the beam loss was dominantly caused by protons generated in the LEBT. This indicates that proton yield could also be an important factor

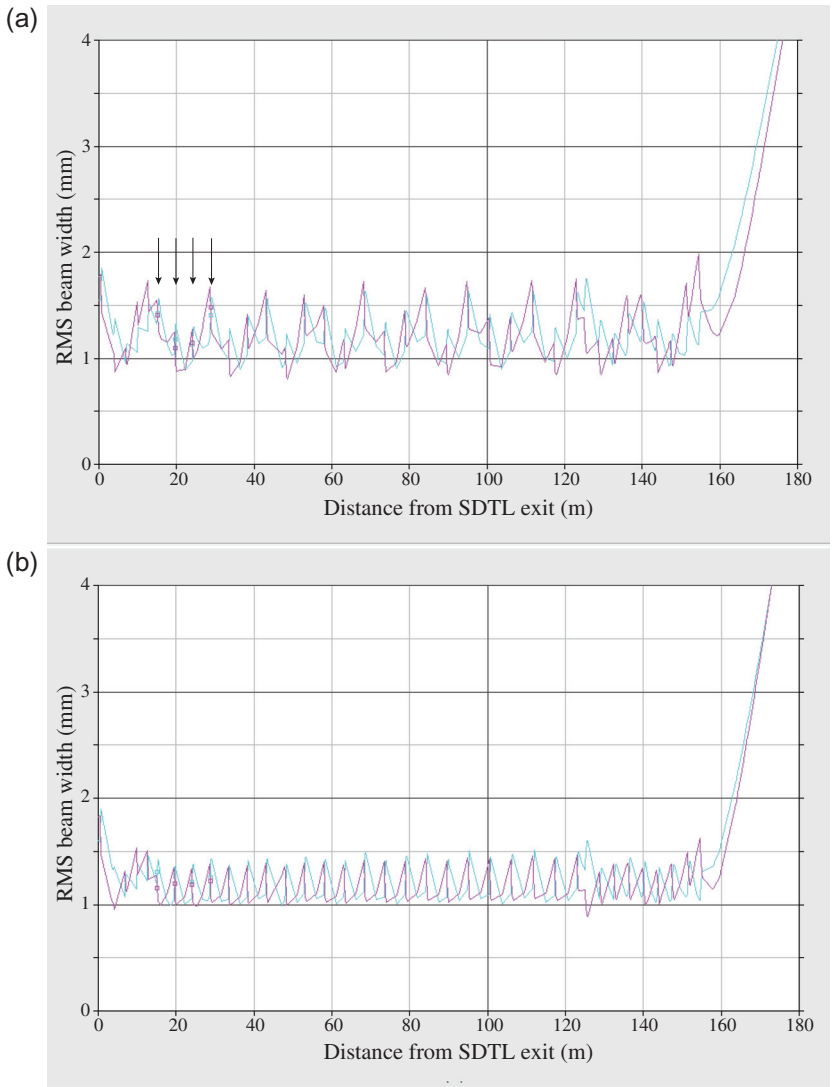

Fig. 5. A result for transverse matching. (a) Before and (b) after transverse matching at the SDTL exit. Blue and red lines respectively show the horizontal and vertical beam envelopes calculated with XAL. The beam envelopes are obtained to fit the measured beam widths varying the Twiss parameters at the SDTL exit. The beam envelope is shown from the SDTL exit to the straight beam dump. The locations of the wire scanners are shown with arrows in (a).

in the LEBT design. It should be noted that the adoption of solenoid focusing in the LEBT could enhance the proton yield, while the generated protons are assumed to be easily diverged away in an alternative electrostatic focusing. This observation and the devised cure provide important information for the design considerations for future high intensity linacs. As the chicane orbit is compatible with beam chopping, we use the proton removal with the chicane orbit in nominal operation.

3.4. Neutral hydrogen loss mitigation

After ramping up the linac beam power to the level of several kW, we noticed a beam loss widely distributed in the straight section after the SDTL. The resultant residual radiation dose is typically 0.6 mSv/h at the beam chamber surface several hours after operation shutdown with a linac beam power of 13.3 kW. As the beam loss monitor signal is not sensitive to the beam orbit correction in its

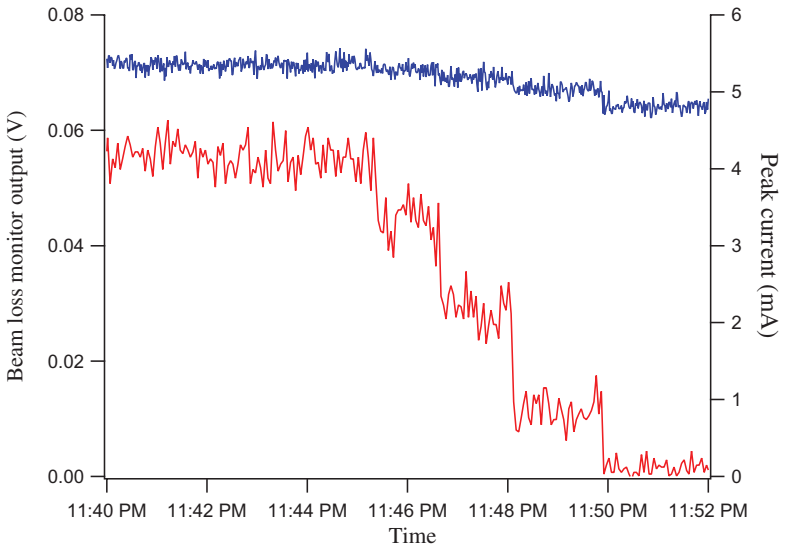

Fig. 6. Variation of the beam loss monitor signal (red) and the peak current (blue) during the experimental demonstration of the effect of proton removal. After setting up the chicane orbit in the MEBT, we started to insert the scraper at about 11:45 PM. The scraper was inserted 4 mm in 1 mm steps. The beam loss signal was measured at the entrance of the first bending magnet, and the peak current was measured at 9 m upstream. The beam loss was drastically reduced with a slight decrease in the beam transmission.

vicinity, we suppose that the beam loss is caused by the neutral hydrogen, or H^0, component generated by single electron stripping in the residual gas scattering of negative hydrogen ions. A GEANT [40] simulation shows that the generated H^0 is likely to hit the chamber wall and be lost after drifting several tens of meters after its generation [41]. Therefore, the observed beam loss is caused by H^0 generated at the downstream part of the SDTL or the upstream part of the straight section after the SDTL. Meanwhile, the yield of H^0 is proportional to the vacuum pressure level at the location of its generation. Thus, a beam experiment was conducted to confirm the above supposition, where the vacuum pumps in the downstream part of the SDTL are turned off while monitoring the beam loss at the downstream straight section [42]. After turning off the vacuum pumps, the vacuum pressure level in the SDTL gradually increased. Analyzing the time evolution of the vacuum pressure level and the beam loss monitor signal, we have tried to identify the correlation between them. After having a linearization calibration for the beam loss monitor signal [39], we have confirmed the linear relation between the beam loss monitor signal and the vacuum pressure level upstream, as seen in Fig. 7. The fitted line can be extrapolated to the zero vacuum pressure level to find the intercept. The ratio between the intercept and the beam loss level with nominal operation provides us with information on the dominance of this loss mechanism. The leftmost marker in Fig. 7 shows the beam loss level with the operating vacuum pressure level. Then, the experimental result shows that the H^0 component generated in the residual gas stripping is the main mechanism for the beam loss in this region. It should be noted that the intercept includes the beam loss caused by H^0 generated in other locations, e.g. the upstream part of the SDTL.

To further confirm the above supposition, we have installed some compact NEG (non-evaporative getter) pumps in the upstream portion of the straight line after the SDTL. After adding the vacuum pumps, the beam loss level in the downstream portion of the straight section has been visibly improved, as seen in Fig. 8, supporting the above supposition on the loss mechanism [42]. This

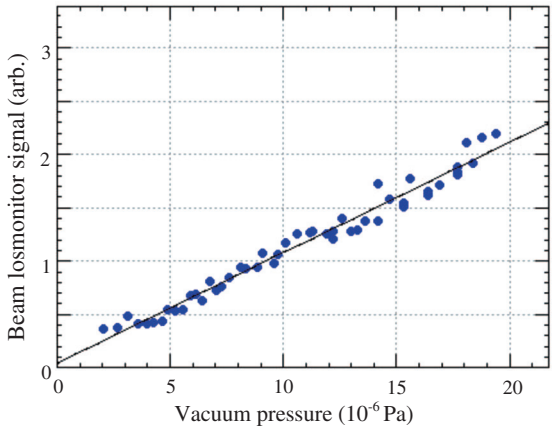

Fig. 7. Experimentally observed correlation between the beam loss monitor signal and the vacuum pressure level. In this plot, the vacuum pressure is measured at the 26th SDTL cavity. Then, the beam loss is measured about 60 m downstream. The marker shows the measured data, and the solid line is the linear fit to it.

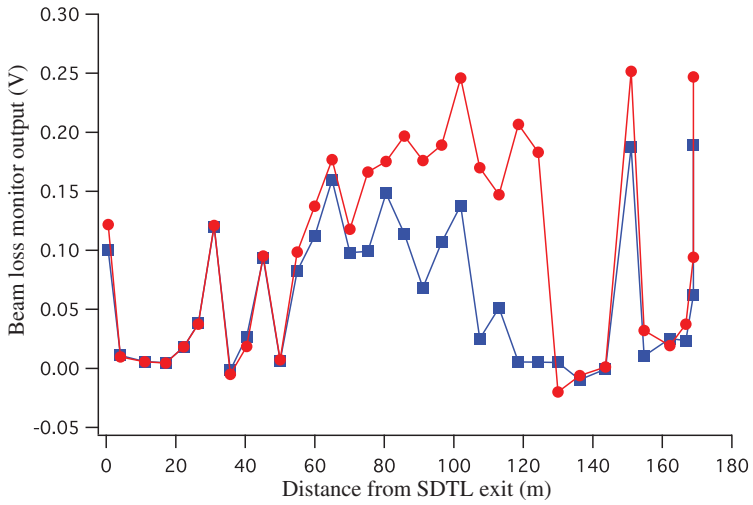

Fig. 8. Beam loss monitor signal level before (red circle) and after (blue square) vacuum improvement with a linac beam power of 7.2 kW. In the improvement, four NEG pumps are added at 51, 73, 83, and 94 m, respectively.

observation indicates that improvement of the vacuum in the downstream part of the SDTL and the upstream part of the future ACS section is important to reduce beam loss in the future ACS section.

As seen in the above subsections, the beam loss mechanisms identified to date in the J-PARC linac are related to electron stripping of negative hydrogen ions. It may be worth remembering here that space-charge effects have been considered to be one of the most probable causes of beam loss in a high intensity linac. However, a beam loss mechanism of this kind has not yet been confirmed in the J-PARC linac.

4. Beam commissioning after the earthquake

We had a magnitude 9.0 earthquake in East Japan in March 2011 followed by a nine-month beam shutdown due to the resultant severe damage [43]. As for the linac, the floor deformation [44] and the damage to the buildings on the ground were particularly severe. Due to the damage, all utilities became unavailable for months. The recovery work involved realignment of almost all beam line

components, including the RF cavities, while realignment of the drift tubes in the DTL and the SDTL has not been conducted. Emphasis was put on swift restoration of beam operation in the adopted realignment scheme [44,45]. In this scheme, the new alignment axis has deflections of up to 1 mrad to smoothly connect to the RCS while avoiding the disassembling of DTL.

After significant restoration efforts, we resumed beam operation of the J-PARC linac in December 2011. After two series of linac beam tuning extending to 14 days in total, we succeeded in resuming user beam operation with a linac beam power of 7.2 kW in January 2012 [46]. The beam power was increased to 13.3 kW in March 2012, which is the same beam power as just before the earthquake. Thus, the situation before the earthquake has been restored in terms of the beam power. While we used deflections in the alignment axis in the realignment, we have seen no obvious effect on the beam quality so far. We have not seen a deterioration of the beam transmission efficiency for the DTL either, which had been a serious concern regarding possible misalignment of the drift tubes inside the DTL tanks. However, we are experiencing unstable behavior of one of the SDTL cavities, which prevents us from operating with nominal RF amplitude. We suppose that the instability is induced by poor surface conditions due to exposure to air of high humidity during some period after the earthquake. The unfavorable effect from the irregular RF setting for the SDTL cavity is currently suppressed by manipulating the RF setting for the neighboring SDTL cavities. With this manipulation, user operation with 13.3 kW is presently sustained with reasonable radiation doses. Although we had a significantly high radiation dose just after the resumption of beam operation, its main cause was identified as misalignment of some beam ducts. After conducting urgent realignment of those beam ducts, the residual radiation dose has gradually decreased and has mostly settled to a level comparable to that before the earthquake.

5. Summary

Beam commissioning of the J-PARC linac started in November 2006, and its user operation began in December 2008. Since then, the beam power from the linac has gradually been increased. As of May 2012, we are operating with a linac beam power of 13.3 kW, which corresponds to an RCS beam power of 200 kW. As we are increasing the beam power to reach the designed linac beam power of 36 kW, we are in a beam commissioning stage while supporting user operation. We divide the beam commissioning into two stages, demarcating the commencement of user operation. In the first stage, the emphasis of the beam commissioning is put on confirming proper functioning of each component and finding adequate basic operation parameters. Meanwhile, the emphasis is shifted to beam power reinforcement in the second stage, where identification of the beam loss mechanism and its mitigation have been increasingly important. In this paper, four topics characteristic of the beam commissioning of high intensity linacs are reviewed. Two of them are regarding beam-based tuning for the most basic operation parameters for the linac, which characterize the first stage of beam commissioning. Meanwhile, the remaining two are studies on beam loss mechanism identification and its mitigation in the second stage of beam commissioning. The beam loss mechanisms identified so far are related to electron stripping of negative hydrogen ions, except for the ones we only experienced after the earthquake. Although there has been a concern that space-charge effects may play an important role in beam loss in the high intensity linac, this kind of beam loss has not yet been confirmed.

After the massive earthquake in March 2011, we resumed beam operation in December 2012 and user operation in January 2012. The linac beam power reached 13.3 kW in March 2012, which is the same beam power as just before the earthquake. Thus, linac operation is restored in terms of beam power. Although we are operating with an irregular setting for some SDTL cavities, the beam

loss level has settled to a level comparable to that before the earthquake. We are currently trying to further reduce the beam loss while preparing for the approaching beam intensity and energy upgrade to realize an RCS beam power of 1 MW.

Acknowledgements

Beam commissioning of the J-PARC linac was conducted by the linac commissioning group with support from all the linac group members. The author would like to acknowledge their devoted contribution. In particular, Dr G. Shen played a pivotal role in the phase–amplitude scan tuning we discussed in Sect. 3.1, Dr H. Sako in the transverse matching in Sect. 3.2 and the proton loss mitigation in Sect. 3.3, and Dr G. Wei in the neutral hydrogen loss mitigation in Sect. 3.4. Also, Dr T. Maruta and Mr A. Miura played central roles in the beam commissioning after the earthquake discussed in Sect. 4. The author would also like to acknowledge that the swift restoration of the J-PARC linac after the earthquake was realized by the great and persistent efforts of all the linac group members, led by Dr H. Oguri, Dr N. Ouchi, and Dr K. Hasegawa.

References

[1] S. Nagamiya, Nucl. Phys. A, **774**, 895 (2006).
[2] Y. Yamazaki (ed.), *Technical Design Report of J-PARC* (KEK Report 2002-13); JAERI-Tech 2003-44.
[3] O. E. Krivosheev and N. V. Mokhov, Proc. ICFA Beam Halo and Scraping Workshop, Lake Como, USA (1999).
[4] G. I. Budker et al., At. Energ., **19**, 507 (1965).
[5] T. Kato, *Proposal of a Separated-type Proton Drift Tube Linac for a Medium-Energy Structure*, KEK Report 92-10 (1992).
[6] S. Fu and T. Kato, Nucl. Instrum. Methods Phys. Res., Sect. A **440**, 296 (2000).
[7] S. Wang, S. Fu, and T. Kato, Nucl. Instrum. Methods Phys. Res., Sect. A, **507**, 305 (2005).
[8] T. Ohkawa, M. Ikegami, J. Qiang, and P. Saha, Nucl. Instrum. Methods Phys. Res., Sect. A, **589**, 1 (2008).
[9] F. Tamura, M. Yamamoto, M. Yoshii, C. Ohmori, M. Nomura, A. Schnase, M. Toda, H. Suzuki, T. Shimada, K. Hara, and K. Hasegawa, Phys. Rev. ST Accel. Beams **12**, 041001 (2009).
[10] T. Ohkawa and M. Ikegami, Nucl. Instrum. Methods Phys. Res., Sect. A, **581**, 606 (2007).
[11] A. Aleksandrov, Proc. LINAC 2010, Tsukuba, Japan (2010), p. 689.
[12] K. Yoshimura, Y. Hashimoto, Y. Hori, Y. Sato, M. Shimamoto, Y. Takeda, M. Uota, Y. Igarashi, H. Nishiguchi, S. Mihara, M. Aoki, N. Nakadozono, and T. Tachimoto, Proc. IPAC 2010, Kyoto, Japan (2010), p. 984.
[13] R. Baartman and D. Yuan, Proc. EPAC 1998, Rome, Italy (1998), p. 949.
[14] H. Oguri, A. Ueno, K. Ikegami, Y. Namekawa, and K. Ohkoshi, Phys. Rev. ST Accel. Beams **12**, 010401 (2009).
[15] H. Ao and Y. Yamazaki, Phys. Rev. ST Accel. Beams **15**, 011001 (2012).
[16] K. Yoshino, E. Takasaki, F. Naito, T. Kato, Y. Yamazaki, K. Tajiri, T. Kawasumi, Y. Imoto, and Z. Kabeya, Proc. LINAC 2000, Monterey, USA (2000), p. 569.
[17] R. A. Jameson, *Equipartitioning in linear accelerators*, Los Alamos National Laboratory Report LA-UR-81-3073 (1981).
[18] M. Reiser and N. Brown, Phys. Rev. Lett. **74**, 1111 (1995).
[19] I. Hofmann and O. Boine-Frankenheim, Phys. Rev. Lett. **87**, 034802 (2001).
[20] M. White, Proc. LINAC 2002, Gyeongju, Korea (2002), p. 1.
[21] L. Arnaudon et al., *Linac4 Technical Design Report*, CERN-AB-2006-084; CARE-Note-2006-022-HIPPI (2006).
[22] H. Danared, M. Eshraqi, W. Hees, A. Jansson, M. Lindroos, S. Peggs, and A. Ponton, Proc. IPAC 2011, San Sebastián, Spain (2011), p. 2631.
[23] M. Ikegami, Proc. 4th Annual Meeting of Particle Accelerator Society of Japan, Wako, Japan (2007), p. 4 (in Japanese).
[24] M. Ikegami, Proc. Hadron Beams 2008, Nashville, Tennessee, USA (2008), p. 333.
[25] M. Ikegami, Proc. LINAC 2008, Victoria, BC, Canada (2008), p. 16.
[26] G. Shen and M. Ikegami, Chin. Phys. C, **33**, 577 (2009).
[27] G. Shen and M. Ikegami, Nucl. Instrum. Methods Phys. Res., Sect. A, **598**, 368 (2009).
[28] J. Qiang, R. D. Ryne, S. Habib, and V. Decyk, J. Comput. Phys. **163**, 434 (2000).

[29] Z. Fang, S. Anami, S. Michizono, S. Yamaguchi, T. Kobayashi, and H. Suzuki, Proc. LINAC 2008, Victoria, Canada (2008), p. 1039.
[30] J. Lagniel, Nucl. Instrum. Methods Phys. Res., Sect. A, **345**, 46 (1994).
[31] J. Lagniel, Nucl. Instrum. Methods Phys. Res., Sect. A, **345**, 405 (1994).
[32] H. Okamoto and M. Ikegami, Phys. Rev. E, **55**, 4694 (1997).
[33] M. Ikegami and H. Okamoto, Jpn. J. Appl. Phys. **36**, 7028 (1997).
[34] T. P. Wangler, K. R. Crandall, R. Ryne, and T. S. Wang, Phys. Rev. ST Accel. Beams **1**, 084201 (1998).
[35] M. Ikegami, S. Lee, Z. Igarashi, H. Akikawa, S. Sato, Y. Kondo, T. Ohkawa, T. Tomisawa, H. Ao, A. Ueno, and K. Hasegawa, Proc. PAC 2005, Knoxville, Tennessee, USA (2005), p. 2750.
[36] H. Sako, A. Ueno, T. Ohkawa, Y. Kondo, T. Morishita, JAEA, Tokai, Japan M. Ikegami, and H. Akikawa, Proc. LINAC 2008, Victoria, BC, Canada (2008), p. 260.
[37] D. Jeon, C. M. Chu, J. Stovall, and S. Assadi, Nucl. Instrum. Methods Phys. Res., Sect. A, **607**, 517 (2009).
[38] C. K. Allen, C. A. McChesney, C. P. Chu, J.D. Galambos, W. D. Klotz, T. A. Pelaia, and A. Shislo, Proc. ICALEPCS 2003, Kyongju, Korea (2003), p. 315.
[39] H. Sako and M. Ikegami, IEEE Trans. Nucl. Sci. **57**, 57 (2010).
[40] J. Allison et al., IEEE Trans. Nucl. Sci. **53**, 270 (2006).
[41] T. Maruta, Proc. IPAC 2011, San Sebastián, Spain (2011), p. 2595.
[42] G. H. Wei, A. Miura, K. Hirano, T. Maruta, and M. Ikegami, Proc. IPAC 2011, San Sebastián, Spain (2011), p. 2598.
[43] K. Hasegawa, M. Kinsho, H. Oguri, and T. Koseki, Proc. IPAC 2011, San Sebastián, Spain (2011), p. 2727.
[44] T. Morishita, H. Asano, and M. Ikegami, Proc. IPAC 2011, San Sebastián, Spain (2011), p. 2601.
[45] M. Ikegami and T. Morishita, Proc. IPAC 2011, San Sebastián, Spain (2011), p. 44.
[46] M. Ikegami, Z. Fang, K. Futatsukawa, T. Miyao, T. Maruta, H. Sako, A. Miura, G. Wei, and J. Tamura, to be published in Proc. IPAC 2012.